PHYSICAL REVIEW B VOLUME 33, NUMBER 11 1 JUNE 1986

Photoemission spectroscopy for the spin-degenerate Anderson model

H. O. Frota* and L. N. Oliveira
Departamento de Física e Ciência dos Materiais, Instituto de Física e Química de São Carlos, Universidade de São Paulo, 13560 São Carlos, São Paulo, Brazil
(Received 17 March 1986)

A procedure that calculates excitation properties for the Anderson model is reported and applied to photoemission. In the mixed-valence regime, hybridized in the ground state, the one- and two-electron impurity configurations generate two spectral resonances. In the Kondo regime, a phenomenological expression describes the narrow peak at the Fermi level.

In the last decade, the computed equilibrium properties[1,2] of dilute magnetic alloys attracted new attention to the Anderson model.[3] Applications of the Hamiltonian to chemisorbing surfaces,[4,5] mixed-valence materials,[6] and heavy fermions[7]—systems outside its original scope—raised interest[8,9] in its excitation properties, featuring particularly the valence and core-level spectral densities.[5,10,11] For large impurity-orbital degeneracy N_f, these[11-13] and other[13] dynamical properties were recently computed. For $N_f=2$, in contrast, only special exact results are available.

We present here a numerical renormalization-group[1] method to calculate excitation properties for spin degeneracy. Applied, as an illustration, to valence photoemission spectroscopy, the procedure tests perturbative results, bridges the gap between the analytically soluble limits $N_f=1$ and $N_f\to\infty$, and, most important, probes the as yet unexplored parametrical half-space mixing in the ground state of the singly and doubly occupied impurity configurations. The resulting twice-resonant spectra mimic the double-humped photoemission curves characteristic of valence fluctuations.[14] Thus, even to the well-documented photoemission problem the computation contributes important quantitative conclusions.

Defined as in Ref. 1, the Anderson Hamiltonian comprises spin-degenerate s-wave conduction states c_k forming a structureless half-filled conduction band, of width 2D, orthogonal to a spin-degenerate impurity state c_f. For occupations $n_f=0$ (configuration f^0), $n_f=1$ (f^1) and $n_f=2$ (f^2), the impurity energies are 0, ϵ_f, and $2\epsilon_f+U$, respectively. A coupling between the conduction and impurity states transfers charge between them at the rate Γ, hybridizing the two f^1 configurations with f^0 and f^2. At zero temperature, the impurity spectral density is

$$\rho_f(\epsilon)=D\sum_F |\langle F|c_f|I\rangle|^2\delta(E_F-E_I-\epsilon) \ , \qquad (1)$$

the factor D making the right-hand side dimensionless; $|I\rangle$ and $|F\rangle$ are the ground state and an excited eigenstate of H_A, with energies E_I and E_F, respectively.

Table I lists the parameters defining four illustrative computer runs for $\rho_f(\epsilon)$. The fixed orbital energy $\epsilon_f=-0.1D$ and transition rate $\Gamma=0.01D\ll|\epsilon_f|$ virtually exclude from the ground state the configuration f^0, unproductive to photoemission. Four interconfigurational gaps[9] $\Delta_+=\epsilon_f+U$, then probe initial occupations ranging from $n_f^0\cong 2$ ($\Delta_+=-0.05D$) to $n_f^0\cong 1$ ($\Delta_+=0.05D$), generally producing two spectral resonances, one for the ground-state impurity configurations f^1, another for the configuration f^2.

In order to interpret the spectra displayed in Fig. 1 we first discuss a trivially soluble limit. For $\Gamma\to 0$, with $\Delta_+>0$ ($\Delta_+<0$), the ground state combines the doubly occupied (singly occupied) impurity with the half-filled, unperturbed conduction band. A single photoemission line of spectral weight two (one), position at $\epsilon_2=-\Delta_+$ ($\epsilon_1=-\epsilon_f$), corresponding to the transition $f^2\to f^1$ ($f^1\to f^0$), then constitutes the inset spectrum in Fig. 1(a) [Fig. 1(c)]. With $\Delta_+=0$, the configurations f^1 and f^2 hybridize and the ground-state impurity occupation n_f^0 equals $\frac{3}{2}$. Two photoemission lines, spectral weights 1 and $\frac{1}{2}$, centers at $\epsilon_2=-\Delta_+$ and $\epsilon_1=-\epsilon_f$, corresponding to the transitions $f^2\to f^1$ and $f^1\to f^0$, respectively, make up the spectrum inserted in Fig. 1(b). For finite Γ, one expects the $f^2\to f^1$ ($f^1\to f^0$) resonance to broaden to a half-width at half maximum Γ (2Γ), proportional to the number of final-state holes[15,16] in the impurity orbital, and shift[16] to the energy $\epsilon_2^*=-\Delta_+^*$ ($\epsilon_1^*=-\epsilon_f-2\Delta_+^*+\Delta_+$), where

$$\Delta_+^*=\Delta_+-(\Gamma/\pi)\ln(\epsilon_f/\Delta_+^*) \ . \qquad (2)$$

This overview accounts for the main features of Fig. 1. For $|\Delta_+|=0.05D$ [Fig. 1(a)], a Lorentzian of area 2, width Γ, central energy $\epsilon_2\cong-\Delta_+^*$ [cf. Eq. (2) and Table I], fits well the calculated $f^2\to f^1$ resonance; since $|\Delta_+|\gg\Gamma$, the $f^1\to f^0$ resonance has insignificant spectral weight, making the expected hump at $\epsilon_1\cong\epsilon_1^*$ imperceptible and making the

TABLE I. Model parameters (ratio Δ_+/Γ), ground-state occupation (n_f^0), and other data extracted from four illustrative computer runs. In all cases, $\Gamma=0.01D$ and $\epsilon_f=-0.1D$. The fitting of the resulting spectra with the smooth curves in Fig. 1 (see text) yields the central energies ϵ_1 and ϵ_2, and the spectral weights S_1 and S_2, of the higher- and lower-energy resonances, $f^1\to f^0$ and $f^2\to f^1$, respectively. The small deviations of n_f^0, computed with less than 1% uncertainty, necessarily equal to the total integrated spectral density, from S_1+S_2 are due to minor features (also reported in Ref. 11) near $\epsilon\cong D$ (not shown in the figure). The remarkably strong $f^2\to f^1$ resonance produces the discrepancies between n_f^0 and n_f^0(phen), Eq. (3), discussed in the text.

Run	Δ_+/Γ	S_1+S_2	n_f^0	n_f^0(phen)	ϵ_1/D	ϵ_2/D
A	−5.0	1.88	1.88	2.00	· · ·	0.053
B1	−0.5	1.63	1.62	1.82	0.123	0.012
B2	0.5	1.43	1.45	1.73	0.118	0.005
C	5.0	1.00	1.05	1.23	0.108	· · ·

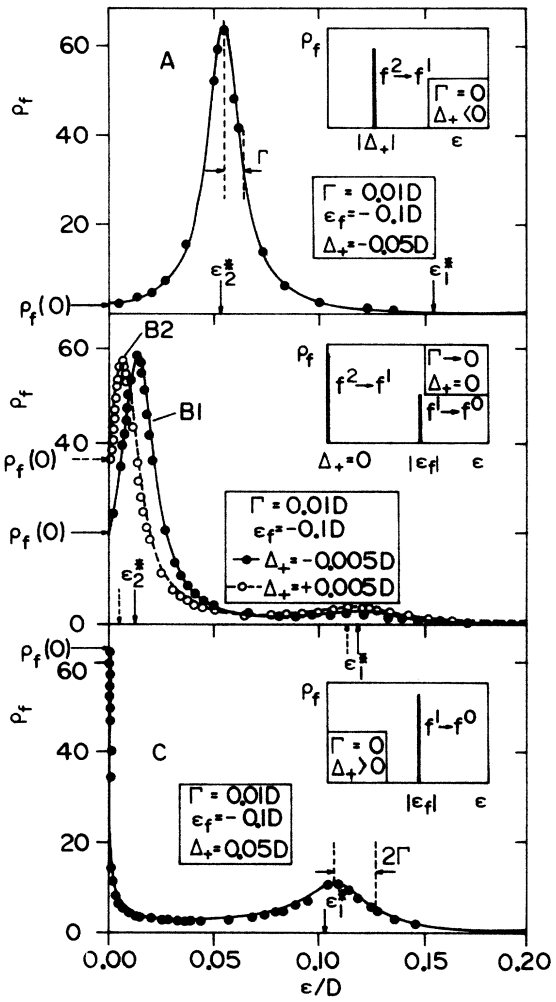

FIG. 1. f-orbital spectral densities (calculated for $\Lambda=3$) for the four parametrical choices in Table I. For each of the runs A, B1, and C (for run B2), a solid (dashed) line fits the calculated densities, shown as filled (open) circles, and a solid (dashed) horizontal arrow points to the static limit, Eq. (5). The vertical arrows indicate the perturbatively calculated (see text) central energies ϵ_1^*, for the $f^1 \rightarrow f^0$, and ϵ_2^* for the $f^2 \rightarrow f^1$ resonances; these resonances are broadened, shifted versions of the photoemission lines constituting the inset ($\Gamma \rightarrow 0$) spectra. The additional, sharp Kondo resonance at $\epsilon=0$ in spectrum C is further discussed in Fig. 2.

spectrum resemble[11] the $N_f=1$ (or $U=0$) spectral density.[10] In contrast, for $|\Delta_+|<\Gamma$, the configurations f^1 and f^2 hybridize strongly in the ground state, and the $f^1 \rightarrow f^0$ resonance grows while the $f^2 \rightarrow f^1$ peak diminishes. For $|\Delta_+|=0.005D$ in particular, which fits accurately the calculated $f^2 \rightarrow f^1$ and $f^1 \rightarrow f^0$ resonances, Fig. 1(b) displays the continuous line B1, a linear combination of two Lorentzians of areas 2 and 1, widths Γ and 2Γ, central energies $\epsilon_2 \cong \epsilon_2^*$ and $\epsilon_1 \cong \epsilon_1^*$ (see Table I), respectively. The linear coefficients, visually adjusted along with the energies ϵ_1 and ϵ_2, yield the spectral weights S_1 and S_2 under the two peaks, respectively. As Table I indicates, these comply well with the sum rule $S_1+S_2=n_f^0$.

Less satisfactory is the agreement between n_f^0 and the phenomenological expression[14] derived by assuming the impurity and conduction band decoupled in the final state. For spin degeneracy, that expression reads

$$n_f^0(\text{phen}) = 1+(1+2S_1/S_2)^{-1} \quad . \tag{3}$$

For $\Delta_+ \rightarrow -\infty$ ($\Delta_+ \rightarrow \infty$), since $n_f^0 \rightarrow 2$ ($n_f^0 \rightarrow 1$) while $S_1 \rightarrow 0$ ($S_2 \rightarrow 0$), Eq. (3) becomes exact, but for $|\Delta_+|=0.005D$, Table I proves it inaccurate. Responsible for the discrepancy are the relatively small binding energies of the $f^2 \rightarrow f^1$ resonance. At such energies, since $\epsilon \lesssim \Gamma$, the final state couples the conduction band strongly to the impurity, hence invalidating Eq. (3).

Albeit based on a crude model, this discussion pertains to the interpretation of photoemission spectra for mixed valence compounds. Since a fluctuating valence requires a transition rate Γ (between configurations f^n and f^{n+1}) larger than the interconfigurational gap Δ_+, the lowest-lying-multiplet resonances must derive their spectral weights from *both* initial configurations, f^n and f^{n+1}. Contrary to the assumption underlying Eq. (3), this conclusion limits (error of 10%, comparable to the discrepancies in Table I) the accuracy[17] of valences extracted from the ratio between spectral weights, S_n/S_{n+1}.

To the run with $\Delta_+=0.005D$ similar considerations apply, yet curve B2 in Fig. 1(b) sets off two differences relative to curve B1: (i) Around the energy ϵ_f, the enhanced $f^1 \rightarrow f^0$ resonance proves the initial configuration f^1 more prominent, and (ii) close to the Fermi level, the inferior fit of the dashed peak (half-width Γ) to the open circles marks a sharper resonance. This incipient narrowing, more intense for larger Δ_+, announces the approaching Kondo[1,2,8,9,11,13] ($n_f^0 \rightarrow 1$) limit.

Representing the Kondo regime, in Fig. 1(c) a spectrum for nearly unitary ground-state occupation shows a spike at zero binding energy, dominating a Lorentzian resonance. The latter is due to the $f^1 \rightarrow f^0$ transition. The former manifests the Kondo effect: Practically excluded from the ground state, the f^2 and f^0 impurity configurations couple virtually to the two f^1 configurations and generate an antiferromagnetic interaction between impurity moment and conduction spins. This produces ultimately a singlet ground state[1,9] and, center at the Fermi level, half-width (proportional[18] to the low-temperature susceptibility, hence easily evaluated[1]) $\Gamma_K=1.1\times10^{-4}D$, a resonance in the conduction band.

To corroborate this interpretation, by showing that the Kondo spike in Fig. 1(c) has half-width Γ_K, Fig. 2 expands the narrow peak and superimposes it on the universal curve

$$\rho_f(\epsilon) = (\tfrac{1}{2}\pi\Gamma)\,\mathrm{Re}[(\epsilon+i\Gamma_K)/i\Gamma_K]^{-1/2} \quad . \tag{4}$$

Here the factors $1/i\Gamma_K$ (within the square brackets) and $\frac{1}{2}\pi\Gamma$ on the right-hand side align the Doniach-Sunjic law,[19,20] $\rho_f \sim E^{-\alpha}$, $\alpha=1-2(\delta/\pi)^2$, for the Fermi-level phase shift[1] $\delta=\pi/2$ and the broadened binding energy $E=\epsilon+i\Gamma_K$, with the exact static limit[8,9,11]

$$\rho_f(0) = (\tfrac{1}{2}\pi\Gamma)\sin^2(\pi n_f^0/2) \quad . \tag{5}$$

The open circles in Fig. 2, calculated for $\Gamma=0.005D$, making Γ_K nearly three orders of magnitude smaller, show that, devoid of adjustable parameters, Eq. (4) describes universally[1] the Kondo limit.

Our numerical approach generalizes the renormalization-group transformation that calculates[1] thermodynamical averages. In Ref. 1, the sequence of conduction energies

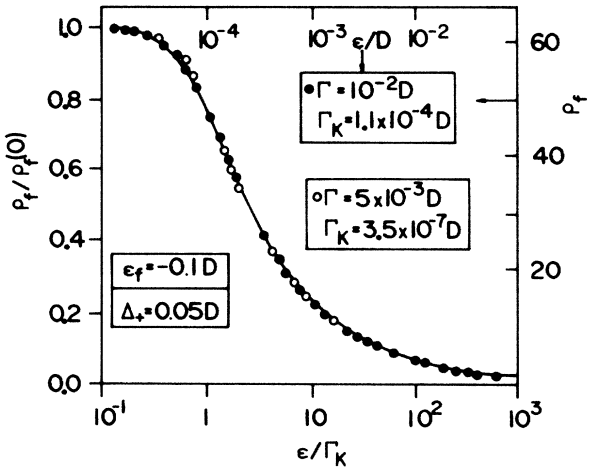

FIG. 2. The Kondo resonance, in reduced spectral density [normalized by $\rho_f(0)$, Eq. (5)] and logarithmic energy (normalized by the Kondo resonance width Γ_K, defined in Ref. 18) scales. The filled circles (absolute scales on the top-horizontal and right-hand vertical axes), obtained by subtracting the Lorentzian $f^1 \rightarrow f^0$ resonance from spectrum 1*C*, correspond to $\Gamma_K = 1.1\times10^{-4}D$; the open circles, calculated for the same ϵ_f and Δ_+, but for $\Gamma = 5\times10^{-3}D$, to $\Gamma_K = 3.5\times10^{-7}D$. Both spectra conform to the universal Eq. (4), a generalized Doniach-Sunjic law represented by the solid line.

$\epsilon_j = \pm D\Lambda^{-j}$ ($j = 0, 1, 2, \ldots, \Lambda > 1$ arbitrary) defines a discrete set of conduction states. Projected onto the basis formed by this set and the impurity states, the Anderson Hamiltonian is made codiagonal and then diagonalized iteratively. The thermodynamical averages over the resulting, discrete eigenvalues are smooth functions of the temperature. In contrast, since the golden-rule energy-conservation relation produces only discrete transition lines—offsprings of the discretized conduction band bearing no resemblance to continuous spectra—this method is inadequate to calculate excitation properties. For quadratic unperturbed Hamiltonians, a straightforward procedure[21] circumvents the difficulty, but for many-body Hamiltonians an alternative formulation is necessary.

We therefore consider the sequence of conduction energies $\epsilon_0 = \pm D$, $\epsilon_j = \pm D\Lambda^{-j-z}$ [$j = 1, 2, \ldots, z \in (-0.5, 0.5)$ fixed arbitrarily]. The prescriptions in Ref. 1 then turn this sequence into a discrete set of conduction states, project the Anderson Hamiltonian onto the basis comprising this set and the impurity states, make it codiagonal,[22] and diagonalize it iteratively. For fixed z, Eq. (1) yields discrete photoemission lines; to produce the continuous spectra in Fig. 1, at each photoemission energy we average (numerically) $\rho_f(\epsilon)$ over z, in the range $-0.5 < z < 0.5$. Equivalent, for single-particle Hamiltonians, to the procedure in Ref. 21, this approach generates, for $U = 0$, at any given frequency, spectral densities differing from the analytical solution[10] by less than 4%. For finite U, the excellent agreement between the horizontal arrows pointing to the exact limit (5) in Fig. 1 and the spectral densities extrapolated to $\epsilon = 0$ evidences good accuracy even at the lowest energies, evaluated in the last iterations[1] of each run, and hence most vulnerable to the accumulated numerical error.

We have described a reliable numerical procedure that calculates excitation properties for the spin-degenerate Anderson model. The computed photoemission spectra cover, for the first time, the parametrical half-space $\epsilon_f < -U/2$, confirm the general conclusions drawn from large-degeneracy calculations,[11-13] and satisfy the relevant exact relations. Equally applicable, at zero or finite temperatures, to such spectroscopies as Mössbauer, x-ray absorption, and bremsstrahlung isochromat, uniformly accurate over the parametrical space, the method presented here provides an important alternative to the large-N_f approach.

The Brazilian Council for Scientific and Technological Development (CNPq) and the Financing Agency for Studies and Projects (FINEP) supported this research.

*Present address: Departamento de Fisica, Universidade do Amazonas, Manaus, AM, Brazil.

[1] H. R. Krishna-murthy, J. W. Wilkins, and K. G. Wilson, Phys. Rev. B **21**, 1003 (1980); **21**, 1044 (1980).

[2] N. Andrei, K. Furuya, and J. H. Lowenstein, Rev. Mod. Phys. **55**, 331 (1983); A. M. Tsvelick and P. B. Wiegmann, Adv. Phys. **32**, 453 (1983).

[3] P. W. Anderson, Phys. Rev. **124**, 41 (1961).

[4] O. Gunnarsson and K. Schönhammer, Phys. Rev. Lett. **41**, 1608 (1978); B. N. J. Persson and R. Ryberg, *ibid.* **48**, 549 (1982).

[5] S.-J. Oh and S. Doniach, Phys. Rev. B **28**, 6606 (1978), and references therein.

[6] See, e.g., *Valence Fluctuations in Solids*, edited by L. M. Falicov, W. Hanke, and M. P. Maple (North-Holland, Amsterdam, 1981).

[7] C. M. Varma, Comments Solid State Phys. **11**, 221 (1985), and references therein; J. W. Allen, S.-J. Oh, L. E. Cox, W. P. Ellis, M. S. Wire, Z. Fisk, J. L. Smith, B. B. Pate, I. Lindau, and A. J. Arko, Phys. Rev. Lett. **54**, 2635 (1985).

[8] F. D. M. Haldane, in *Valence Fluctuations in Solids*, edited by L. M. Falicov, W. Hanke, and M. P. Maple (North-Holland, Amsterdam, 1981), p. 153; R. M. Martin, Phys. Rev. Lett. **48**, 362 (1982).

[9] J. W. Wilkins, opening talk in *Valence Instabilities*, edited by P. Watcher and H. Boppart (North-Holland, Amsterdam, 1982), and references therein.

[10] W. Brenig and K. Schönhammer, Z. Phys. **267**, 201 (1974); K. Schönhammer and O. Gunnarsson, Phys. Rev. B **18**, 6606 (1978).

[11] O. Gunnarsson and K. Schönhammer, Phys. Rev. Lett. **50**, 604 (1983); Phys. Rev. B **28**, 4315 (1983); **28**, 7330 (1983); O. Gunnarsson, K. Schönhammer, D. D. Sarma, F. U. Hillebrecht, and M. Campagna, *ibid.* **32**, 5499 (1985).

[12] P. Coleman, Phys. Rev. B **29**, 3035 (1984).

[13] N. E. Bickers, D. L. Cox, and J. W. Wilkins, Phys. Rev. Lett. **54**, 230 (1985), summarize previous large-N_f results; see also F. Patthey, B. Delley, W.-D. Schneider, and Y. Baer, Phys. Rev. Lett. **55**, 1518 (1985).

[14] See, e.g., G. K. Wertheim, W. Eib, E. Kaldis, and M. Campagna, Phys. Rev. B **22**, 6240 (1980).

[15] L. H. Hirst, Phys. Rev. Lett. **35**, 1394 (1975); also, Refs. 11-13 report a width $N_f\Gamma$ for the $f^1 \rightarrow f^0$ resonance.

[16] The perturbative treatment of the deviations from the valence fluctuation fixed point, described in Ref. 1, calculates the central energies and widths of the $f^1 \rightarrow f^0$ and $f^2 \rightarrow f^1$ resonances; see also F. D. M. Haldane, Phys. Rev. Lett. **40**, 416 (1978); **40**, 911(E) (1978); and Ref. 11.

[17] See M. Campagna, in *Valence Fluctuations in Solids*, edited by L. M. Falicov, W. Hanke, and M. P. Maple (North-Holland, Am-

sterdam, 1981), p. 23, and ensuing discussion.

[18]L. N. Oliveira and J. W. Wilkins, Phys. Rev. Lett. **47**, 1553 (1981).

[19]S. Doniach and M. Sunjic, J. Phys. C **3**, 285 (1970).

[20]As discussed in Ref. 12, the $1/N_f$ expansion washes out infrared divergences, hence producing a different law. Experimental results nonetheless often follow a Doniach-Sunjic law. See G. K. Wertheim and P. H. Citrin, in *Topics in Applied Physics,* edited by M. Cardona and L. Ley, Lecture Notes in Physics, Vol. 26 (Springer, Berlin, 1978), p. 197.

[21]L. N. Oliveira and J. W. Wilkins, Phys. Rev. B **24**, 4863 (1981); D. L. Cox, H. O. Frota, L. N. Oliveira, and J. W. Wilkins, *ibid.* **32**, 555 (1985).

[22]In Ref. 1, for large n, the nth codiagonal element approaches $\Lambda^{-n/2}$; here it approaches $\Lambda^{-z-n/2}$.